ACS NANO

www.acsnano.org

ARTICLE

Biomimetic Heterodimerization of Tetrapeptides to Generate Liquid Crystalline Hydrogel in A Two-Component System

Bihan Wu, Shuang Zhao, Xuejiao Yang, Laicheng Zhou, Yang Ma, Hongyue Zhang, Wenbin Li, and Huaimin Wang*

Cite This: *ACS Nano* 2022, 16, 4126–4138

Read Online

ACCESS | Metrics & More | Article Recommendations | Supporting Information

ABSTRACT: **Anisotropic structures made by hierarchical self-assembly and crystallization play an essential role in the living system. However, the spontaneous formation of liquid crystalline hydrogel of low molecular weight organic molecules with controlled properties remains challenging. This work describes a rational design of tetrapeptide without N-terminal modification and chemical conjugation that utilizes intermolecular interactions to drive the formation of nanofiber bundles in a two-component system, which could not be accessed by a single component. The diameter of nanofibers can be simply controlled by varying the enantiomer of electrostatic pairs. Mutation of lysine (K) to arginine (R) results in an over 30-fold increase of mechanical property. Mechanistic studies using different techniques unravel the mechanism of self-assembly and formation of anisotropic liquid crystalline domains. All-atom molecular dynamics simulations reveal that the mixture of heterochiral peptides self-assembles into a nanofiber with a larger width compared to the homochiral assemblies due to the different stacking pattern and intermolecular interactions. The intermolecular interactions show an obvious increase by substituting the K with R, facilitating a more stable assembly and further altering the assembly mechanics and bulk material properties. Moreover, we also demonstrated that the hydrogel properties can be easily controlled by incorporating a light-responsive group. This work provides a method to generate the liquid crystalline hydrogel from isotropic monomers.**

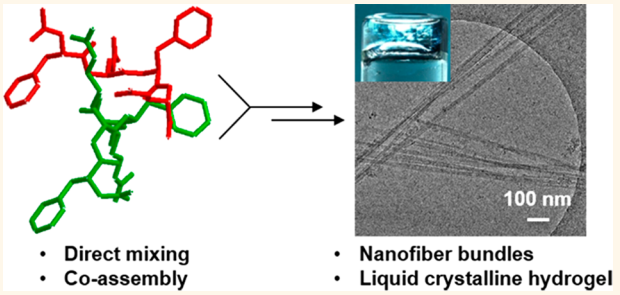

KEYWORDS: *peptide, two-component hydrogel, hierarchical self-assembly, liquid crystalline hydrogel, intermolecular interactions*

INTRODUCTION

Biological systems contain a lot of examples of materials that are formed by anisotropic structures, which play an essential role in the living system to carry out particular functions. For example, anisotropic extracellular matrix plays an essential role in determining cell proliferation, migration, and survival in health and disease conditions.[1,2] Articular cartilage exhibits anisotropic microstructural organization when subjected to tension.[3] Anisotropic organization of actin and myosin in the muscle sarcomere functions in muscle contraction.[4] Inspired by these natural phenomena and the understanding of the interactions between cellular activities and materials at the genetic and molecular levels, significant progress has been made to fabricate biomimetic scaffolds for tissue engineering and regenerative medicine using natural or synthetic materials.[5−9] Hydrogels are an important class of this type soft materials due to the biomimetic property and high water contents (>90%). Although anisotropic hydrogels on the macroscopic scale have been successfully achieved in several polymeric hydrogels via directional stimuli, such as magnetic electric fields, shear forces, thermal pathway, and ionic strength, anisotropic supramolecular hydrogels that consist of the nanofibrous network through self-assembly of small molecules (MW < 2000) have attracted growing attention in recent years.[10−13]

Although in the past few decades it was feasible to form a supramolecular hydrogel through molecular self-assembly, most supramolecular hydrogels explored so far are limited to isotropic property.[14,15] Among these items, peptide and amino

Received: November 7, 2021
Accepted: February 25, 2022
Published: March 1, 2022

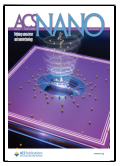

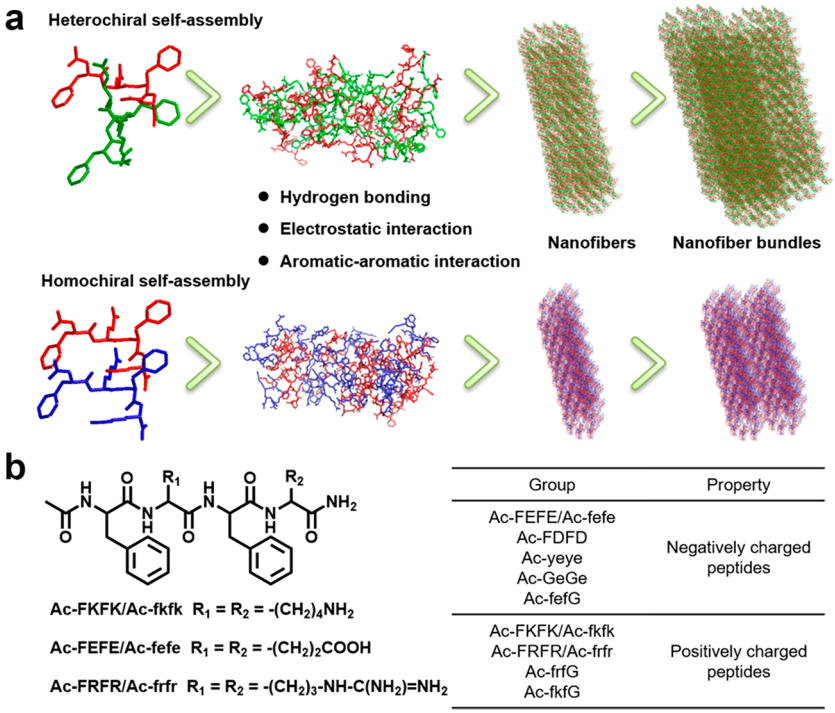

Figure 1. (a) Illustration of the nanofiber bundle formations by tetrapeptides. (b) Molecular structure of tetrapeptides and the list of major tetrapeptide sequences explored within this study.

acid derived self-assembly systems have been extensively designed and studied due to their various advantages and applications.[16−27] Typically, short peptide-based hydrogels contain 3D random entangled nanofibers, resulting in isotropic hydrogels in most reported works. Recent works suggested that those nanofibers further formed anisotropic higher-ordered assemblies and nanoscale crystals, which could be aligned by external forces to exhibit macroscopic anisotropic properties. For example, Van Esch and co-workers used the chemical-gradient (pH-gradient) method to direct alignment of fibers within minutes.[28] The Van Hest[29] and Adams[30] groups applied magnetic field to induce the alignment of nanofibrous assemblies formed by peptide amphiphile. Stupp and co-workers recently reported a monodomain hydrogel aligned by shear force. The liquid crystal of filaments could serve as a bridge to direct cells spatially for function.[31,32] Xu and co-workers recently integrated aromatic−aromatic interactions and enzyme-instructed self-assembly to induce the formation of aligned supramolecular hydrogel.[33] Despite the success of these works, progress toward the formation of anisotropic structures made by spontaneous hierarchical self-assembly and crystallization has been limited and remains challenging because most external stimuli and incorporating of capping group (e.g., naphthalene and alkyl chains) could induce cytotoxicity against living cells.[34−41] For example, Stupp and co-workers[34] demonstrated that less cohesive assemblies of peptide amphiphiles caused disruption of the cell membrane and contact-mediated cell death. The cell viability was rescued by increasing intermolecular hydrogen bonding, decreasing the alkyl tail length or removing one charged residue.

Here, we reported that controlling the intermolecular interaction of two oppositely charged small molecules (e.g., tetrapeptide, MW < 700 Da) without hydrophobic modification affords spontaneously aligned nanofiber bundles and biocompatible hydrogels in pH 7.4 aqueous solution (Figure 1a). We found that a single component of molecules dissolves very well in the aqueous solution (pH 7.4) without detectable assemblies and nanostructures by dynamic light scattering (DLS) and transmission electron microscopy (TEM). However, the mixture of the oppositely charged components forms a nanofibrous hydrogel. The diameter of the nanofibers and the mechanical properties could be simply controlled by varying the enantiomer of electrostatic pairs and the single amino acid in one component, respectively. Detailed mechanistic studies by TEM, cryogenic transmission electron microscopy (Cryo-TEM), atomic force microscope (AFM), circular dichroism (CD), Fourier transform infrared (FTIR), nuclear Overhauser effect spectroscopy (NOESY), wide-angle X-ray scattering (WAXS), and polarized optical microscopy (POM) reveal the self-assembly mechanism and the formation of anisotropic liquid crystalline domains within the hydrogel. All-atom molecular dynamics (MD) simulations reveal that the mixture of heterochiral peptides self-assembles into a nanofiber with a larger width compared to the homochiral assemblies. The intermolecular interactions show an obvious increase by substituting the lysine (K) with arginine (R). Coarse-grained MD simulations demonstrate the role of electrostatic interactions for driving fibrous cluster formation. Moreover, we demonstrated the programmable ability of our system by light. This work illustrates an efficient approach for generating aligned nanofibrous soft materials with controllable properties according to the emerging need of structural anisotropy in biomimetic application, such as tissue engineering, cell culture, mass transport, and regenerative medicine.[42,43]

RESULTS AND DISCUSSION

Molecular Design and Self-Assembly. Gazit and co-workers[44] have explored the self-assembly property of dipeptide (phenylalanine-phenylalanine, FF), which has attracted increasing interest in the last few decades.

https://doi.org/10.1021/acsnano.1c09860
ACS Nano 2022, 16, 4126−4138

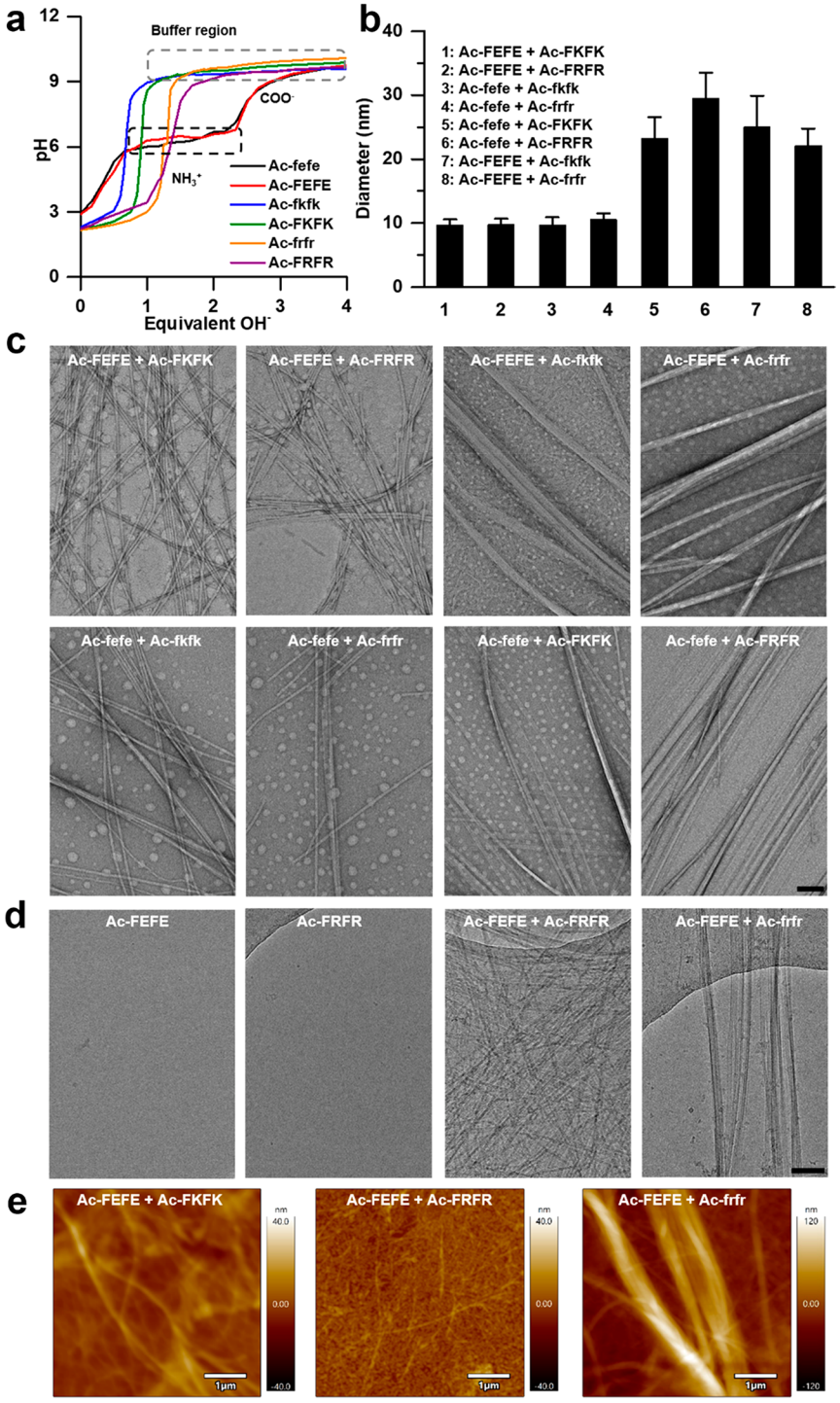

Figure 2. (a) Titration curves for tetrapeptides at a concentration of 5.0 mM. The 0.1 M NaOH is titrated into aqueous solution. (b) The diameter of the nanofibers (n = 30). Data are depicted as mean ± SD. (c) TEM images of the mixture of peptides (10.0 mM) in aqueous solution (pH 7.4) after 4 days of incubation. Scale bar, 100 nm. (d) Cryo-TEM images of the single component of peptide and the mixture of peptides (10.0 mM) in aqueous solution (pH 7.4) after 4 days of incubation. Scale bar, 100 nm. (e) AFM images of the mixture of peptides (10.0 mM) in aqueous solution (pH 7.4) after 4 days of incubation. Scale bar, 1 μm.

Incorporation of the hydrophobic motif with an external stimulating group (e.g., light, pH, or enzyme sensitive group) and D-amino acid are often necessary to generate hydrogels of short peptides, which restricts their future applications by synthetic complexity, biocompatibility of stimuli, and scalability.[45] Very recently, two-component hydrogel formed by mixing solutions of ultrashort (less than five amino acids) peptides without heating or the addition of other stimuli is a convenient strategy among the peptide-based biomaterials, and the properties of which go beyond conventional single-component hydrogel.[46−48] Moreover, the alternating sequence of hydrophobic and charged amino acids is usually employed in the self-assembled long peptides' scaffold.[49−51] Inspired by the fact that electrostatic effects provide the most important

https://doi.org/10.1021/acsnano.1c09860
ACS Nano 2022, 16, 4126−4138

energy contribution in the formation of protein complexes and protein functions[52,53] and repetitive patterns found in the sequence of natural fibrous proteins (such as tropoelastin and fibroin),[54,55] we rationally designed tetrapeptide with the alternating feature of nonpolar aromatic F and charged amino acids. The negatively charged peptides contain F and glutamic acid (E), and positively charged peptides are composed of F and K or R residues (Figure 1b). We synthesized all peptides by standard Fmoc-based solid-phase peptide synthesis (SPPS) using a rink amide resin to yield a C-terminal amide, and used N-terminal acetylation to avoid additional ionization (the lowercase letters mark the D-amino acids). The structure, purity, and molecular weight of peptides are confirmed by liquid chromatography−mass (LC-MS) and proton nuclear magnetic resonance (^{1}H NMR) (Figures S1 and S2).

We titrated 0.1 M sodium hydroxide (NaOH) into a 5.0 mM solution of tetrapeptide to test the buffering region and the respective charges (Figure 2a).[56] At pH value below the buffering region, **Ac-FEFE/Ac-fefe** peptide forms a white precipitate and turns into a clear solution at pH 7.0 due to the deprotonation of the carboxyl group. The titration curves of **Ac-FKFK/Ac-fkfk** and **Ac-FRFR/Ac-frfr** peptide show a buffering region where the pH is near 10.0. The protonated forms of **Ac-FKFK/Ac-fkfk** and **Ac-FRFR/Ac-frfr** peptide are predominate at the physiological pH.

Gelation requires the hierarchical assembly from molecule to continuous network structure.[57] We next examined the gelation ability of tetrapeptide at pH 7.4 aqueous solution, where all groups are expected to be charged. The peptide at the concentration of 10.0 mM is readily soluble at neutral pH. The solution of the single component of tetrapeptide could not form a hydrogel after 4 days of incubation at room temperature because of the electrostatic repulsion (Figure S3). Upon mixing of the oppositely charged **Ac-FEFE/Ac-fefe** and **Ac-FRFR/Ac-frfr** peptide in aqueous solution (pH 7.4, 20.0 mM), an opaque hydrogel forms within 5 min (Figure S4). The mixture of heterochiral **Ac-FEFE/Ac-fefe** and **Ac-fkfk/Ac-FKFK** peptide forms a hydrogel rapidly (within 5 min), while the mixture of homochiral (all-L or all-D) enantiomers of tetrapeptide forms a hydrogel more slowly (>8 h, Figure S4). All of the mixtures of the oppositely charged system form hydrogels after 4 days of incubation at the concentration of 10.0 mM. The hydrogels formed by the mixture of homochiral **Ac-FEFE/Ac-fefe** and **Ac-FRFR/Ac-frfr** peptide appear more translucent compared with those prepared from the mixture of heterochiral **Ac-FEFE/Ac-fefe** and **Ac-frfr/Ac-FRFR** peptide (Figure S5). At lower concentration (6.5 mM and 5.0 mM), only the mixture of heterochiral **Ac-FEFE/Ac-fefe** and **Ac-frfr/Ac-FRFR** peptide forms a hydrogel after 4 days of incubation (Figures S6 and S7). These results indicate that the gelation process is kinetically controlled by concentration and intermolecular interactions of tetrapeptides.

A turbidity kinetics assay can give the dynamic self-assembly property of the resulting hydrogel (Figure S8). The results show that the optical density (OD) values of the mixture of **Ac-FEFE/Ac-fefe** and **Ac-FKFK/Ac-fkfk** peptide show negligible changes within 180 min. The absorbance of the mixture of heterochiral **Ac-FEFE/Ac-fefe** and **Ac-frfr/Ac-FRFR** peptide starts to increase after mixing and reaches an OD of 0.2 after 180 min due to the quick self-assembly of the peptide. Compared to the heterochiral peptide, a delay in self-assembly is observed for the mixture of the homochiral **Ac-FEFE/Ac-fefe** and **Ac-FRFR/Ac-frfr** peptide. These results indicate that the mixture of peptides spontaneously forms assemblies in water and larger assemblies form in the mixture of heterochiral peptides than the homochiral ones, possibly due to the phenomenon of stereocomplexation and the molecular orientation of heterochiral peptides.[58] The fast increase and higher OD values in the R-containing tetrapeptide are due to the additional hydrogen bonding from the guanidyl group and its multiple binding with the carboxyl group.

We next explored the influence factors in the hydrogel formation. As shown in Figure S9, a dipeptide of **Ac-fe**, **Ac-FR**, **Ac-fr**, the mixture of oppositely charged dipeptides, and the mixture of an oppositely charged dipeptide and a tetrapeptide could not form a hydrogel at aqueous solution (pH 7.4). The tetrapeptide with a free carboxyl group at the C-terminal fails to form a hydrogel in the mixture system (Figure S10), suggesting the importance of the C-terminal amidation. Moreover, the acetylation/amidation increases the hydrophobicity of peptides and generates peptides more closely mimicking the native protein, as evidenced by the calculated log P (octanol−water partition coefficient) values of tetrapeptides (Table S1). All of the solutions of mixture of **Ac-FEFE/Ac-fefe** and **Ac-FKFK/Ac-fkfk** peptide (10.0 mM) fail to form a stable hydrogel at pH 12.0 (Figure S11), where the charges of the positive peptide are eliminated because of the excess of pK_a of K,[59] indicating that the formation of a hydrogel correlates to the protonation of amino groups. The pH of the solution does not change dramatically on salt addition (1.0 M NaCl). The addition of NaCl screens the charges of peptide and results in a weak and unstable hydrogel formed by the mixture of **Ac-FEFE** and **Ac-FKFK/Ac-fkfk** peptide because of a loss of the ionic cross-links.[60,61] The mixture of **Ac-FEFE** and **Ac-FRFR/Ac-frfr** peptide forms a hydrogel in the presence of 1.0 M NaCl possibly due to strong hydrogen bonding interactions within the nanofibers (Figure S12). We synthesized several other peptides (Scheme S2) where the one K/E/R residue is substituted with glycine (G), limiting the total charge. The results show that the mixture of peptide bearing only one charged residue could not form a hydrogel (Figure S13). The substitution of tyrosine (Y) or G for F within the tetrapeptide, which tends to be more polar because of the hydroxyl group of Y and more hydrophilic because of the lack of an aromatic group than F, fails to provide sufficient interactions to form the hydrogel (Figure S14). The replacing of E in **Ac-FEFE** with aspartic acid (D) results in tetrapeptide with less hydrophobicity and fails to form a stable hydrogel in the two-component system (Table S1 and Figure S15). These results indicate that the repetitive sequence of the peptide, the configuration of an amino acid, the ionic and aromatic−aromatic interactions, and the hydrophilic−hydrophobic balance together influence the final properties of hydrogels and the nanostructures during the self-assembling process. We therefore further investigated the structural and mechanical properties of hydrogels.

Morphologies of Hydrogels. We could hardly observe any structures in a single peptide solution by TEM analysis (Figure S16). To further explore whether the single component could form assemblies, we performed the DLS experiment. The DLS count rates (Figure S17) of solutions of single component peptide (10.0 mM) are very low (less than 12 kcps), indicating no detectable assemblies in the sample. Figure 2b,c indicates that the hydrogels contain nanofibers and nanofiber bundles. The diameters of nanofibers assembled by the mixture of L-peptides are about 10 nm, while the mixture of

https://doi.org/10.1021/acsnano.1c09860
ACS Nano 2022, 16, 4126−4138

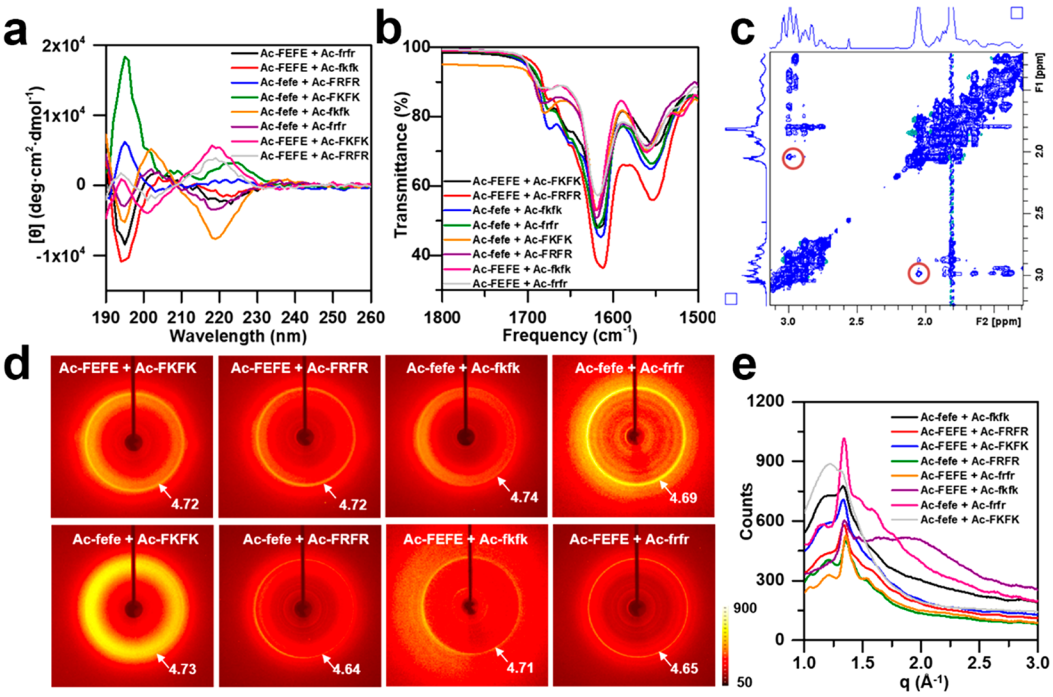

Figure 3. (a) CD spectra of diluted hydrogels (0.3 mM) in aqueous solution (pH 7.4). Molar ellipticities ([θ]) are measured as a function of wavelength. (b) FTIR absorbance spectra of hydrogels (10.0 mM). (c) NOESY spectrum of the mixture of Ac-FEFE and Ac-FRFR peptide (10.0 mM in 10% D_2O). Close contact is indicated by the red circle. (d) Debye rings of WAXS patterns from hydrogels (10.0 mM) in aqueous solution (pH 7.4) after 4 days of incubation. (e) The integrated spectra of WAXS pattern plotted as a function of the scattering vector q.

D-peptides behaves in a similar manner. The mixture of heterochiral tetrapeptides results in larger diameter nanofibers. Specifically, the mixture of the tetrapeptide pair shows a hierarchical self-assembly process from nanofibers to multifibrous alignment bundles, which could be due to the fiber−fiber interactions resulting from the complementary charge surface of nanofibers. The extent of bundling for the mixture of heterochiral tetrapeptides is more obvious than other groups and consistent with the observation for opacity of the hydrogel. To preclude the drying effect,[62] we also obtained Cryo-TEM images of solutions of the single component peptide and samples of the mixture of representative peptides. The results show that the mixture of **Ac-FEFE** and **Ac-frfr** peptide comprises bundled nanofibers with an average diameter of about 25 nm, whose width is larger than those of the mixture of **Ac-FEFE** and **Ac-FRFR** peptide (Figure 2d). AFM images further demonstrate the structural evolution from nanofibers to oriented nanofiber bundles. The mixture of heterochiral enantiomers of the tetrapeptide forms bundled nanofibers, while the mixture of homochiral peptides consists of fewer multifibrous alignment bundles (Figure 2e). These results suggest that the diameter of the nanofiber could be modulated by changing the enantiomer of electrostatic pairs. Unlike the other two-component supramolecular hydrogels,[46,63,64] where molecules could self-assemble and form hydrogels individually, we demonstrated the coassembly of two oppositely charged tetrapeptides after mixing and the higher-order structure formation only started from two independent solutions of monomers.

Conformation of Hydrogels. To investigate the structure of self-assemblies, we examined the solutions and hydrogels by CD and attenuated total reflectance (ATR) FTIR. CD spectra show that the mixture of **Ac-FEFE** and **Ac-FKFK/Ac-FRFR** peptide exhibits a characteristic minimum near 198 nm and a maximum at 220 nm. The spectrum of the mixture of **Ac-fefe** and **Ac-fkfk/Ac-frfr** peptide exhibits a maximum and a minimum that is essentially the opposite from that of the L-peptide pair. Similarly, the mixture of **Ac-FEFE** and **Ac-fkfk/Ac-frfr** peptide displays a positive maximum around 198−205 nm and a negative band at 220 nm, while the mixture of **Ac-fefe** and **Ac-FKFK/Ac-FRFR** peptide shows a mirror image of their enantiomeric pair. The spectra reveal that the mixture of tetrapeptides has a random coil secondary structure (Figure 3a).[65] Although CD spectra show that the mixture of tetrapeptides has a random coil structure, we could not preclude the possibility of the formation of higher-order nanofibers. The large Cotton effect at about 220 nm in the single-component solution (Figure S18a) originates from the peptidic backbone. The subsequent decrease of the intensity in the two-component hydrogel indicates that the association of the oppositely charged pair results in electrostatic interaction to reduce the CD signals. We recorded the FTIR spectra of all samples at the amide I (1600−1700 cm^{-1}, C═O stretching vibration) and amide II (1500−1600 cm^{-1}, N−H bending and C−N stretching vibrations) regions (Figure 3b). Before mixing, **Ac-FEFE/Ac-fefe** peptide exhibits ionized carboxyl groups at neutral pH, evidenced by a strong peak around 1552−1562 cm^{-1} indicative of the asymmetric carboxylate COO^- band stretching vibration, and no significant absorption at 1710 cm^{-1} where protonated acid group COOH absorbs (Figure S18b).[66] The sharp peak at 1670 cm^{-1} is consistent with stretches for TFA counterions.[64] Amide I is sensitive to a secondary structure and is related to the backbone conformation for different hydrogen bonding environments. The mixture of peptides presents a stretching band at around

https://doi.org/10.1021/acsnano.1c09860
ACS Nano 2022, 16, 4126−4138

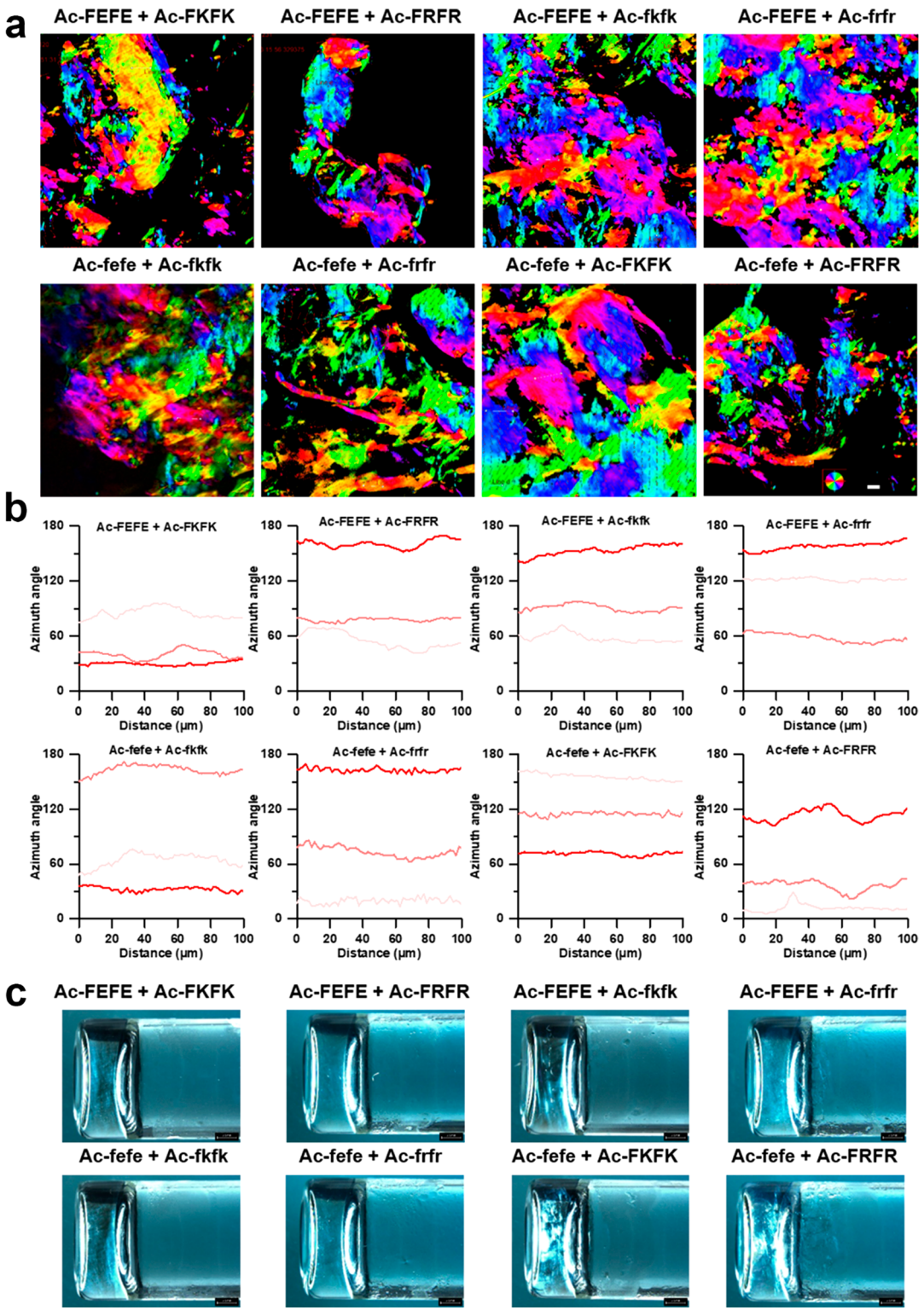

Figure 4. (a) POM images of hydrogels (10.0 mM) in aqueous solution (pH 7.4) after 4 days of incubation. The colored circle indicates the azimuth of slow axis orientation. Scale bar, 100 μm. (b) Analysis of the azimuth angle of hydrogels using lines (n = 3, 100 μm). (c) Macroscopic photographs of hydrogels (10.0 mM) by POM. Scale bar, 2.5 mm.

1650 cm^{-1}, which is assignable to a random coil structure as the major feature.[67,68]

Coassembly of Peptides. Further insight into molecular arrangement and stacking of nanostructures is gained by NOESY and WAXS. The ^{1}H NMR, correlation spectroscopy (COSY), heteronuclear single-quantum correlation spectroscopy (HSQC), and rotating frame NOE spectroscopy (ROESY) experiment are acquired for the single component peptide (**Ac-FEFE**, **Ac-FRFR**) because of the medium-sized molecular weight to determine the assignments of protons and interatomic distances (Figure S19 and Table S2). In contrast to the single component peptide, the chemical shifts in the ^{1}H

https://doi.org/10.1021/acsnano.1c09860
ACS Nano 2022, 16, 4126−4138

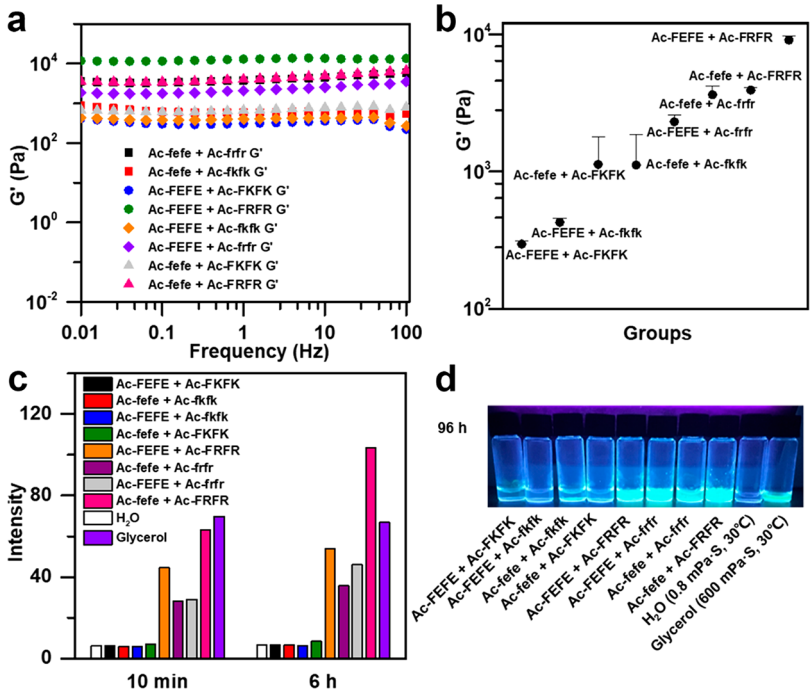

Figure 5. (a) The G' of hydrogels (10.0 mM) and (b) summary of G' of different hydrogels at frequency 1 Hz under a strain of 1.0%. Data are depicted as mean ± SD. (c) The emission (516 nm) of the mixture of peptides (10.0 mM) with fluorescent reporter (1.0 μM). Excitation: 375 nm. The H_2O and glycerol are used as a negative control and a positive control, respectively. (d) Optical images of the mixture of peptides (10.0 mM) with fluorescent reporter (1.0 μM) after 96 h incubation.

NMR spectrum of the mixture of **Ac-FEFE** and **Ac-FRFR** peptide have no noticeable variation (Figure S20). A close contact (<5 Å) between the H_γ protons of E and the H_δ protons of R emerges in the NOESY spectrum of the mixture of **Ac-FEFE** and **Ac-FRFR** peptide (Figure 3c), demonstrating the coassembly of two peptides within the fibers.[69] These scattering rings reveal amorphous phase and highly disordered stacking of peptides in the WAXS patterns. The Debye rings with different *d*-spacing correspond to the crystallographic planes in materials.[70] The hydrogel shows one clear scattering peak corresponding to 4.7 Å in *d*-spacing ($\mathbf{q}$ = 1.3 Å^{-1}), suggesting the −N−H···O═C− hydrogen bonding (Figure 3d,e).[71,72] The WAXS patterns of the single component of peptide show the same scattering peak but with much lower intensity than that observed at the mixture of peptides, indicating a loss of structure (Figure S21). The results show that the hydrogen bonding interactions play an essential role in driving the self-assembly. Taken together, these results support that the electrostatic interaction of hydrophilic motif, aromatic−aromatic interaction, and hydrogen bonding synergistically provide the driving forces to trigger the coassembled process.

Birefringence of Hydrogels. Anisotropic materials (such as crystals and aligned polymers) lead to a refractive index changing with the polarization of the light, the difference of which is defined as the birefringence.[73] Polarized optical images provide detailed information on birefringence at the fibrillar level. The orientation pseudo images display the degree of polarization and the polarization azimuth angle in hydrogels (Figure 4a). The hydrogel formed from the mixture of peptides contains highly birefringent domains, indicating the anisotropic property of nanofiber bundles, whereas the solution of single component peptide hardly shows any birefringence (Figure S22). We measured the azimuth angle and retardance of hydrogels using lines (n = 3, 100 μm). The distribution of the azimuth angle in birefringent regions is largely uniform, indicating that hydrogels contain some linear aligned structures (Figure 4b). The gray scale images represent anisotropy in the sample measured as the magnitude of retardance, where the black and white area in the image represent zero retardance and maximum retardance value, respectively (Figure S23). The images exhibit multiple domains with a magnitude of retardance between 0 and 80 nm, confirming the highly birefringent domains in the hydrogel.[73] We also studied the macroscopic properties of hydrogel by POM (Figure 4c and Figure S24). The aligned structures exhibit birefringence and appear as bright areas in an otherwise dark background. The hydrogels formed by the mixture of heterochiral tetrapeptides have largely uniform alignment to result in significant birefringence, while those formed by the mixture of homochiral enantiomers of tetrapeptide exhibit less birefringence and consist of fewer multifibrous alignment bundles in low-magnification TEM images (Figure S25) and AFM images (Figure S26). Those nanofiber bundles in hydrogels have uniform and aligned orientations in the mesoscopic scale but not throughout the hydrogel. According to Onsager's theory, the parallel arrangement in solution results in the minimum excluded volume and the entropy maximum of the total system, thus facilitating the isotropic−anisotropic phase separation.[74] The POM results indicate the spontaneous Onsager transition from nanofibers to nanofiber bundles and liquid crystalline phase in hydrogel. The stacking of heterochiral peptide and electrostatic interactions could promote the interfiber interactions between nanofibers. The resultant enhancement of interfiber contacts could be a reliable approach to induce the formation of nanofiber bundles and thus generate birefringence in hydrogels.

https://doi.org/10.1021/acsnano.1c09860
ACS Nano 2022, 16, 4126−4138

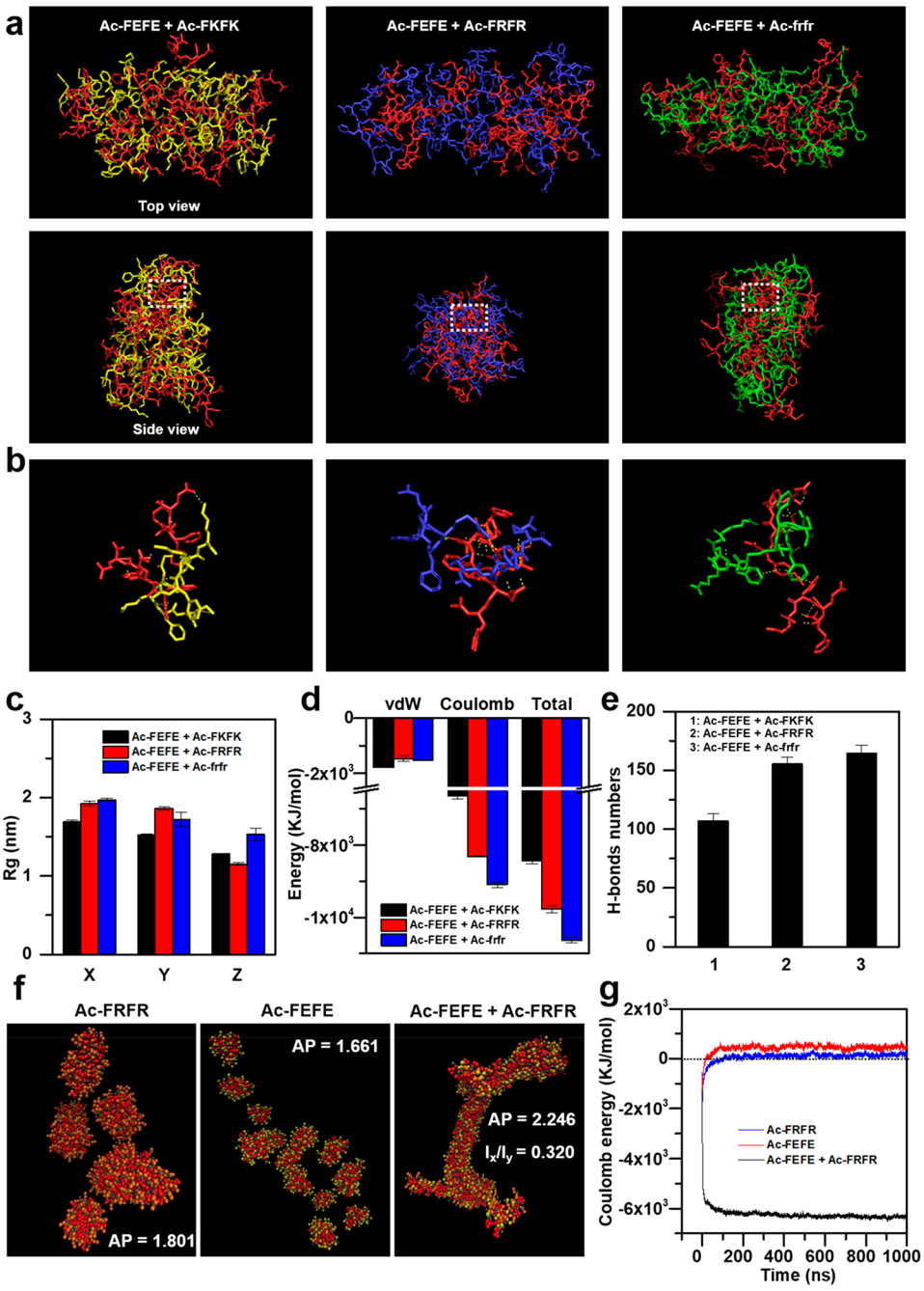

Figure 6. (a) All-atom MD simulations of the self-assembly of catanionic peptides shown in top view and side view. Red, Ac-FEFE; green, Ac-frfr; blue, Ac-FRFR; yellow, Ac-FKFK. (b) Representative stacking patterns of the mixture of catanionic peptides. The dash lines indicate the hydrogen bonds and π-interactions. (c) The values of Rg of aggregates. (d) van der Waals force, coulomb energy, and total energy of systems at the end of the simulation. (e) The number of hydrogen bonds of three systems. (f) Coarse-grained MD simulations of Ac-FRFR, Ac-FEFE, and the mixed Ac-FEFE and Ac-FRFR systems. Molecular structure, AP value, and I_x/I_y value after self-assembly of three systems. Red beads, F; orange beads, R; yellow beads, E; gray beads, capping groups. (g) The coulomb energy of three systems.

Mechanical Properties of Hydrogels. We performed the rheological measurement to evaluate the viscoelastic behavior of these hydrogels at the same concentration. We performed the linear viscoelastic regime of the hydrogels by a strain sweep to determine the proper shear force for the dynamic frequency sweep of a hydrogel. The values of the storage modulus (G') of the two-components are larger than their loss modulus (G'') and show a weak dependence of strain from 0.1% to 10.0%, indicating the formation of a hydrogel. In contrast, the values of G' of a single molecule are almost the same with the G'', suggesting that the single component can only form liquidlike solution (Figure S27). We next used dynamic frequency sweep to study the mechanical property of hydrogels at different oscillation frequencies at a constant oscillation amplitude. Figure 5a shows that all hydrogels have negligible frequency dependence (with G' dominating G''), suggesting the formation of an effective and viscoelastic hydrogel of two components. The G' (295.9 ± 14.7 Pa) of **Ac-FEFE + Ac-FKFK** is the lowest among the groups, suggesting the weakest hydrogel within all of the tested groups. Surprisingly, mutation

https://doi.org/10.1021/acsnano.1c09860
ACS Nano 2022, 16, 4126−4138

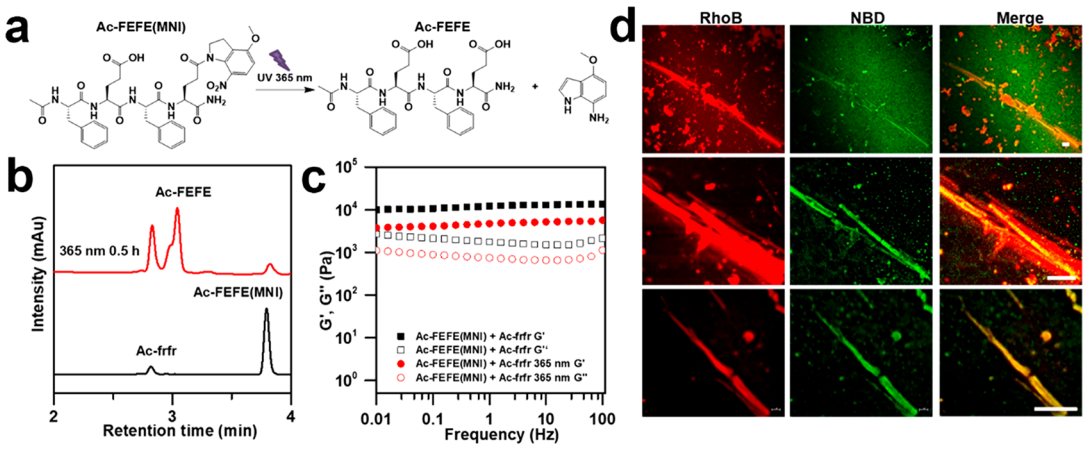

Figure 7. (a) Photolysis reaction of Ac-FEFE(MNI). LC-MS spectra (b) and the mechanic property (c) of the mixture of Ac-FEFE(MNI) and Ac-frfr peptide (10.0 mM) before and after irradiation with 365 nm light. (d) Confocal laser scanning microscope images of the mixture of peptides (Ac-fefe, 5.0 mM; Ac-frfr, 4.5 mM; NBD-frfr, 0.5 mM; RhoB-fefe, 0.02 mM, 50 μL) after 12 h incubation. Scale bar, 10 μm.

of K to R results in the most rigid hydrogel. The G' (9087.3 ± 603.6 Pa) of **Ac-FEFE** + **Ac-FRFR** is over 30-fold greater than the original hydrogel and is comparable with the mechanical property of the polymeric hydrogel (e.g., polypeptide[75]) at a similar concentration (Figure 5b). We further investigated the effects of the rate of gelation, the chirality of peptides, and the viscosity of hydrogel on mechanical property. The results show that the mixture of peptides (10.0 mM) forms hydrogel with a different rate of gelation (Table S3). The mutation of K to R results in rapid gelation (within 2 h) of all of the tested groups. The time-dependent rheological experiments of the mixture of **Ac-FEFE**/**Ac-fefe** and **Ac-FRFR**/**Ac-frfr** peptide (Figure S28) provide qualitative information about the gel formation. The G' is higher than G'' and reaches a plateau after approximately 600 s, indicating the kinetics formation of a stable hydrogel. The mixture of heterochiral **Ac-FEFE**/**Ac-fefe** and **Ac-fkfk**/**Ac-FKFK** peptide shows much faster gelation than the mixture of homochiral enantiomers (Figure S29). After 4 days of incubation, the characteristics of the mixture of **Ac-FEFE**/**Ac-fefe** and **Ac-FKFK**/**Ac-fkfk** peptide do not change significantly, which reveals that the mechanical properties do not depend on the rate of gelation and the chirality of peptide. We next compared the viscosity of the mixture of peptides using a boron-dipyrromethene (BODIPY)-based fluorescent reporter (Figure S30) whose C−C bond between the phenyl and BODIPY can freely rotate to produce fluorescence quenching in a low-viscosity environment.[76] It could offer enhanced fluorescence in highly viscous media because the rotation is restricted. The emission of BODIPY (516 nm) is considerably increased over time in the mixture of **Ac-FEFE**/**Ac-fefe** and **Ac-FRFR**/**Ac-frfr** peptide, indicating the increased solvent viscosity (Figure 5c,d). The mixture of peptides results in higher-viscosity solution and more hydrogel with enhanced mechanical properties by altering the amino acid K to R, regardless of configuration, which is possibly due to the multiple binding orientations between guanidinium and carboxylate.[77] The results indicate that the mechanical properties of the hydrogel can be easily controlled by intermolecular interactions in tetrapeptides.

MD Simulations. We performed the all-atom MD simulations to investigate the assembly of the building blocks into ordered structures and the differences in intermolecular interactions. All-atom MD results reveal that the mixture of peptides shows a rapid assembly, as indicated by the rapid decrease of solvent accessible surface areas (SASA) during the assembly process (Figure S31). The mixture of peptides mainly self-assembles into disordered fiber-shaped aggregates and occupies conformation similar to the experimental results (Figure 6a). The representative stacking patterns of three systems show that the mixture of heterochiral peptides forms loosely packed aggregates (Figure 6b). The radius of gyration (Rg) of Z is defined as the distribution of atoms around Z-axis and represents the diameter of fiber. In the homochiral assemblies, the Rg is almost unaffected by the substitution of K with R. In contrast, nanofiber with different Rg is formed due to the different initial configuration of the peptide. Compared to the homochiral peptides, the larger Rg of the mixture of **Ac-FEFE** and **Ac-frfr** peptide suggests that the mixture of heterochiral peptides self-assembles into an aggregate with a larger width (Figure 6c). We calculated the intermolecular noncovalent interactions of three systems (Figure 6d,e). The balance of noncovalent interactions results in the formation of different structures. The hydrogen bonds are reported to direct the fibrillation process, whereas van der Waals interactions and electrostatic forces are involved in the further interfiber interactions.[74] The mixture of **Ac-FEFE** and **Ac-frfr** peptide forms a more stable structure with different pattern from the homochiral assemblies, as evidenced by enhanced coulomb energy, lower total energy, and a larger number of hydrogen bonds. The coulomb energy and the number of hydrogen bonds show an obvious increase by substituting the K with R, regardless of the configuration (Figure 6d,e). The enhanced intermolecular interactions facilitate a more stable assembly and further alter the assembly mechanics and bulk material properties, which are consistent with the results of the mechanical property.

We also performed coarse-grained MD simulations (Figure S32) to understand the self-assembly of the larger size. The aggregation propensity (AP) is defined as the ratio of initial SASA after energy minimization to the final SASA after the self-assembly process and is used to quantify the level of aggregation of peptides.[78] For morphology analysis, the moments of inertia (I) along the principal axes of the largest cluster of the mixed **Ac-FEFE** and **Ac-FRFR** system after equilibration are calculated. A cluster with $I_x \approx I_y$ shows a spherical structure, while $I_x < I_y$ indicates a fibrous shape. The

https://doi.org/10.1021/acsnano.1c09860
ACS Nano 2022, 16, 4126−4138

mixed system shows a larger AP value than that of the single peptide with an I_x/I_y value of 0.320, indicating that the mixed two-component system is easier to aggregate and form a fibrous cluster (Figure 6f). Figure 6g shows that the coulomb energies between the peptides in both **Ac-FEFE** and **Ac-FRFR** systems are positive, because of electric charges of the same sign. In contrast, the coulomb interaction energy in a mixed **Ac-FEFE** and **Ac-FRFR** system has a negative and large value because of the attractive interactions of the **Ac-FEFE** and **Ac-FRFR** molecules. These computational data are consistent with the results that are observed by TEM and DLS. The electrostatic interaction between **Ac-FEFE** and **Ac-FRFR** peptides provides the driving force for enhanced aggregation behavior in a mixed peptide system.

Programming the Property of Hydrogel. Using external stimuli to program the mechanical property of the hydrogel spatiotemporally attracted growing interest in recent years. Although stimuli-responsive biomaterials in one component hydrogel have been extensively studied, controlling the self-assembly properties in multicomponent hydrogel remains less explored.[79] To demonstrate the spatiotemporal program of our hydrogel, a photocaged E, namely 4-methoxy-7-nitroindolinyl glutamic acid [E(MNI)], which has been applied in a caged neurotransmitter along with the initiation of gel−sol phase transition of one-component hydrogel,[80] is used to replace the E in the **Ac-FEFE**, resulting in **Ac-FEFE(MNI)** (Figure 7a). The results show that the mixture of **Ac-FEFE(MNI)** with **Ac-frfr** peptide generates hydrogel much faster than the original pair because of the introduction of hydrophobic group (Figure S33). LC-MS spectra indicate that the irradiation of 365 nm light could release the negatively charged glutamate side-chain within 0.5 h (Figure 7b). The rheological data suggests that the G' value of hydrogel after irradiation by ultraviolet (UV) light decreases from 12 133.9 to 4755.7 Pa, indicating hydrogel's mechanical property could be controlled locally by light. To explore the applications of our system, we intend to apply the coassembly of peptide with orthogonal function using fluorescence-labeled peptides as a model. NBD and Rhodamine B, models of two functional groups, are used as substitutes for the Ac group to prepare the **NBD-frfr** and **RhoB-fefe**, respectively (Scheme S3 and Figure S34). The coassembly of **NBD-frfr**, **RhoB-fefe**, **Ac-frfr**, and **Ac-fefe** forms nanofiber bundles, which exhibit both green fluorescence from NBD and red fluorescence from RhoB, indicating the orthogonal property in nanofiber bundles (Figure 7d). Thus, we envision that the platform developed in this work could facilely modulate nanofibers with other orthogonal functions.[42]

CONCLUSION

This work illustrates a rational design of two complementary charged tetrapeptides without hydrophobic modification to produce a series of liquid crystalline hydrogels. The experimental results and MD data reveal that the changes of phase behavior and differences in mechanical properties rely on intermolecular interactions and the chirality of the peptide. We demonstrated that liquid crystalline hydrogel can be formed spontaneously by charge-complementary pairs of designed native tetrapeptides, which start from two independent solutions of monomers. Detailed studies suggest that the morphological outcome of such a phenomenon depends on the surface charges, hydrogen bond, and molecular orientation of heterodimers/homodimers of peptides. The morphologies of complementary heterochiral peptides are larger than the corresponding homochiral pairs of peptides, consisting of large nanofiber bundles. Morphologies obtained from self-assembled complementary charged tetrapeptides and MD simulations suggest that the aggregates of molecules exhibit the geometrical anisotropy, which promotes the alignments of nanofibers to form liquid crystalline microdomains in the hydrogel. The concentration-dependent formation of liquid crystalline hydrogel suggests the formation of a lyotropic liquid crystal in our system. For hydrogel formation, the results suggest that complementary heterochiral pairs of peptides tend to aggregate and result in fast gelation. Mutation of K to R in the tetrapeptide results in enhanced mechanical property of the hydrogel, which is due to multiple binding orientations of the guanidyl group with the carboxyl group. The *in vitro* cytotoxicity experiments also show that the mixture of peptide has negligible toxicity on cell proliferation (human bone osteosarcoma Saos-2 cells and marrow stromal HS-5 cells, Figure S35), indicating the biocompatibility of the hydrogels. Moreover, we could easily incorporate a light-sensitive motif to modulate the mechanic property of the resulted hydrogel and introduce orthogonal functions, suggesting the programmable ability of our system.

MATERIALS AND METHODS

Synthesis of Peptide. We prepared all peptides by SPPS on rink amide resin (Hecheng Science & Technology CO., Ltd. China). Fmoc deprotection was carried out using 20% piperidine in *N*,*N*-dimethylformamide (DMF) solution. The peptide was acetylated and then cleaved using a solution of trifluoroacetic acid (TFA)/triisopropylsilane (TIS)/water (95%/2.5%/2.5%) cocktail for 2 h. The cleaved peptide was evaporated in vacuo to remove excess TFA and precipitated in cold diethyl ether. The product was purified using high-performance liquid chromatography (HPLC, Agilent, U.S.A.) using a reverse phase C18 column (Waters, RP18 10.0 μm, 19 × 150 mm) with acetonitrile (CH_3CN, 0.1% of TFA) and water (0.1% of TFA) as the eluents. The flow rate was 10 mL/min and the process was monitored by UV absorbance at 220 and 254 nm. The pure product was combined and lyophilized. The peptide was characterized by LC-MS (Agilent, U.S.A.) spectra and ^{1}H NMR (Bruker BioSpin, Switzerland) spectra. The log P values of tetrapeptides were calculated using Molinspiration (https://www.molinspiration.com/).

Hydrogel Formation. We dissolved the peptide in water separately at 20.0, 10.0, 6.5, and 5.0 mM and adjusted the pH to 7.4 with 0.1 M NaOH by pH meter. The solutions of positively charged peptide and negatively charged peptide at equal volume were combined and vortexed to form mixed-component gels. The mixture of peptide was prepared by the same method at the concentration of 20.0 mM (20.0 mM in total, 10.0 mM of each peptide), 10.0 mM (5.0 mM of each peptide), 6.5 mM (3.25 mM of each peptide), and 5.0 mM (2.5 mM of each peptide).

TEM and Cryo-TEM. For TEM, the hydrogel (10 μL) was placed on 200 mesh carbon-coated copper grids and incubated for 1 min. Excess solution was removed using filter paper. The sample was stained with 2% (w/v) uranyl acetate (10 μL) solution and imaged on Talos L120C TEM with an accelerating voltage of 120 kV (Thermo Fisher, Netherlands). The diameter (n = 30) was analyzed using ImageJ. A line that is perpendicular to nanofiber was drawn manually to measure the width of nanofiber. For cryo-TEM, the sample (4 μL, 10.0 mM) was applied to the UV/ozone treated graphene grids (Quantifoil 300 mesh) in Vitrobot Mark IV (Thermo Scientific, Netherlands). The grid was blotted against filter paper and rapidly plunged into liquid ethane for the vitrification. The sample was transferred to liquid nitrogen and imaged on Glacios TEM operated at 200 kV (Thermo Scientific, Netherlands).

AFM. The morphology was examined by Cypher ES Environmental AFM (Oxford Instruments, US). The hydrogel (10.0 mM, 10 μL) was spread over the surface of the silicon substrate and hydrated.

https://doi.org/10.1021/acsnano.1c09860
ACS Nano 2022, 16, 4126−4138

All AFM experiments were carried out at room temperature. The topographical AFM images were scanned over areas of 20 × 20 μm^2 and 5 × 5 μm^2.

POM. The hydrogel (10.0 mM, 50 μL) was placed on a microscope glass slide and imaged on Oosight Imaging System (Hamilton Thorne, U.S.A.) equipped with polarization optics and a differential interference contrast (DIC) module (Olympus IX73, Japan). Three lines were drawn manually to analyze the azimuth angle and retardance in images. The azimuth angle (0−180° from the horizontal orientation) refers to the orientation of the slow axis and describes the orientation of material. The light polarized parallel to the slow axis and fast axis experience the highest refractive index (the slowest travel) and lowest refractive index (the fastest travel), respectively. Retardance $R = (n_e - n_o)\cdot d$, where n_e is extraordinary refractive index, n_o is ordinary refractive index, and d is the thickness of the birefringent material.[33,73] The macroscopic photographs of hydrogel (10.0 mM, 300 μL) were taken by Leica M205 C POM (Germany).

Rheology. The hydrogel (10.0 mM, 500 μL) was prepared in a 5 mL plastic syringe with the top removed and Parafilm covered. The gel was loaded into the rheometer from the syringe by pushing the plunger after 4 days of incubation.[79] The rheological test was performed on ARES-G2 rheometer (TA-Waters, US) with an upper plate diameter of 25 mm using a 0.45 mm gap height at 25 °C. The strain scan was performed from 0.1% to 100% with a frequency of 1 Hz. The frequency sweep was performed at the range of 0.01 to 100 Hz under a strain of 1.0%. We performed each experiment three individual times, and the final data represent the average of the three tests with standard deviation. The time-dependence of the G' and G'' was measured at a fixed frequency of 1 Hz and a fixed strain amplitude of 1.0% using a 0.45 mm gap height at 25 °C.

ASSOCIATED CONTENT

Supporting Information

The Supporting Information is available free of charge at https://pubs.acs.org/doi/10.1021/acsnano.1c09860.

Details on experimental procedures and additional characterization including details of peptide synthesis and characterization, log P values, LC-MS spectra, NMR spectra; optical images, TEM images, AFM images, POM images of hydrogels; CD spectra, FTIR spectra, DLS test, rheological experiments, turbidity study, viscosity test, and *in vivo* cytotoxicity of peptides (PDF)

AUTHOR INFORMATION

Corresponding Author

Huaimin Wang − *Key Laboratory of Precise Synthesis of Functional Molecules of Zhejiang Province, School of Science, Institute of Natural Sciences, Westlake Institute for Advanced Study, Westlake University, Hangzhou 310024 Zhejiang Province, China;* orcid.org/0000-0002-8796-0367; Email: wanghuaimin@westlake.edu.cn

Authors

Bihan Wu − *Key Laboratory of Precise Synthesis of Functional Molecules of Zhejiang Province, School of Science, Institute of Natural Sciences, Westlake Institute for Advanced Study, Westlake University, Hangzhou 310024 Zhejiang Province, China*

Shuang Zhao − *Key Laboratory of 3D Micro/Nano Fabrication and Characterization of Zhejiang Province, School of Engineering, Institute of Advanced Technology, Westlake Institute for Advanced Study, Westlake University, Hangzhou 310024 Zhejiang Province, China*

Xuejiao Yang − *Key Laboratory of Precise Synthesis of Functional Molecules of Zhejiang Province, School of Science, Institute of Natural Sciences, Westlake Institute for Advanced Study, Westlake University, Hangzhou 310024 Zhejiang Province, China*

Laicheng Zhou − *Key Laboratory of Precise Synthesis of Functional Molecules of Zhejiang Province, School of Science, Institute of Natural Sciences, Westlake Institute for Advanced Study, Westlake University, Hangzhou 310024 Zhejiang Province, China*

Yang Ma − *Key Laboratory of Precise Synthesis of Functional Molecules of Zhejiang Province, School of Science, Institute of Natural Sciences, Westlake Institute for Advanced Study, Westlake University, Hangzhou 310024 Zhejiang Province, China*

Hongyue Zhang − *Key Laboratory of Precise Synthesis of Functional Molecules of Zhejiang Province, School of Science, Institute of Natural Sciences, Westlake Institute for Advanced Study, Westlake University, Hangzhou 310024 Zhejiang Province, China*

Wenbin Li − *Key Laboratory of 3D Micro/Nano Fabrication and Characterization of Zhejiang Province, School of Engineering, Institute of Advanced Technology, Westlake Institute for Advanced Study, Westlake University, Hangzhou 310024 Zhejiang Province, China;* orcid.org/0000-0002-1240-2707

Complete contact information is available at: https://pubs.acs.org/10.1021/acsnano.1c09860

Author Contributions

H.M.W. conceived this work. B.H.W. performed the experiments and collected data. S.Z. performed some MD experiments and collected data under the supervisor of W.B.L. X.J.Y., Y.M., H.Y.Z., and L.C.Z. synthesized and characterized some of compounds. B.H.W. and H.M.W. analyzed the data and wrote the manuscript with the input from the other authors. All authors read and approved the manuscript. All authors have given approval to the final version of the manuscript.

Notes

The authors declare no competing financial interest.

ACKNOWLEDGMENTS

This project was supported by the National Natural Science Foundation of China (82022038), foundation of Westlake University and Tencent Foundation. S.Z. and W.L. thank the support by NSFC under Project No. 62004172, Westlake Multidisciplinary Research Initiative Center (MRIC) under Award No. 20200101 and Westlake University HPC Center. We thank the Instrumentation and Service Center for Molecular Sciences, Instrumentation and Service Center for Physical Sciences, General Equipment Core Facility, and Biomedical Research Core Facilities at Westlake University for the assistance with measurements.

REFERENCES

(1) Mouw, J. K.; Ou, G. Q.; Weaver, V. M. Extracellular Matrix Assembly: A Multiscale Deconstruction. *Nat. Rev. Mol. Cell Biol.* **2014**, *15* (12), 771−785.

(2) Park, D.; Wershof, E.; Boeing, S.; Labernadie, A.; Jenkins, R. P.; George, S.; Trepat, X.; Bates, P. A.; Sahai, E. Extracellular Matrix Anisotropy Is Determined by TFAP2C-Dependent Regulation of Cell Collisions. *Nat. Mater.* **2020**, *19* (2), 227−238.

(3) Hossain, M. J.; Noori-Dokht, H.; Karnik, S.; Alyafei, N.; Joukar, A.; Trippel, S. B.; Wagner, D. R. Anisotropic Properties of Articular Cartilage in An Accelerated *in Vitro* Wear Test. *J. Mech. Behav. Biomed. Mater.* **2020**, *109*, 103834.
(4) Huxley, A. F. Muscular Contraction. *J. Physiol.* **1974**, *243* (1), 1−43.
(5) Li, Y.; Xiao, Y.; Liu, C. The Horizon of Materiobiology: A Perspective on Material-Guided Cell Behaviors and Tissue Engineering. *Chem. Rev.* **2017**, *117* (5), 4376−4421.
(6) Brown, T. E.; Anseth, K. S. Spatiotemporal Hydrogel Biomaterials for Regenerative Medicine. *Chem. Soc. Rev.* **2017**, *46* (21), 6532−6552.
(7) Wang, H.; Leinwand, L. A.; Anseth, K. S. Cardiac Valve Cells and Their Microenvironment-Insights from *in Vitro* Studies. *Nat. Rev. Cardiol.* **2014**, *11* (12), 715−727.
(8) Webber, M. J.; Appel, E. A.; Meijer, E. W.; Langer, R. Supramolecular Biomaterials. *Nat. Mater.* **2016**, *15* (1), 13−26.
(9) Dou, X.; Mehwish, N.; Zhao, C.; Liu, J.; Xing, C.; Feng, C. Supramolecular Hydrogels with Tunable Chirality for Promising Biomedical Applications. *Acc. Chem. Res.* **2020**, *53* (4), 852−862.
(10) Babu, S. S.; Praveen, V. K.; Ajayaghosh, A. Functional π-Gelators and Their Applications. *Chem. Rev.* **2014**, *114* (4), 1973−2129.
(11) Sano, K.; Ishida, Y.; Aida, T. Synthesis of Anisotropic Hydrogels and Their Applications. *Angew. Chem., Int. Ed.* **2018**, *57* (10), 2532−2543.
(12) Park, S. S.; Urbach, Z. J.; Brisbois, C. A.; Parker, K. A.; Partridge, B. E.; Oh, T.; Dravid, V. P.; Olvera de la Cruz, M.; Mirkin, C. A. DNA- and Field-Mediated Assembly of Magnetic Nanoparticles into High-Aspect Ratio Crystals. *Adv. Mater.* **2020**, *32* (4), 1906626.
(13) Hu, Y.; Lin, R.; Zhang, P.; Fern, J.; Cheetham, A. G.; Patel, K.; Schulman, R.; Kan, C.; Cui, H. Electrostatic-Driven Lamination and Untwisting of β-Sheet Assemblies. *ACS Nano* **2016**, *10* (1), 880−888.
(14) Estroff, L. A.; Hamilton, A. D. Water Gelation by Small Organic Molecules. *Chem. Rev.* **2004**, *104* (3), 1201−1218.
(15) Ulijn, R. V.; Jerala, R. Peptide and Protein Nanotechnology into The 2020s: Beyond Biology. *Chem. Soc. Rev.* **2018**, *47* (10), 3391−3394.
(16) Du, X.; Zhou, J.; Shi, J.; Xu, B. Supramolecular Hydrogelators and Hydrogels: From Soft Matter to Molecular Biomaterials. *Chem. Rev.* **2015**, *115* (24), 13165−13307.
(17) Ulijn, R. V.; Smith, A. M. Designing Peptide Based Nanomaterials. *Chem. Soc. Rev.* **2008**, *37* (4), 664−675.
(18) Zhang, S. G. Fabrication of Novel Biomaterials through Molecular Self-Assembly. *Nat. Biotechnol.* **2003**, *21* (10), 1171−1178.
(19) Gazit, E. Self-Assembled Peptide Nanostructures: The Design of Molecular Building Blocks and Their Technological Utilization. *Chem. Soc. Rev.* **2007**, *36* (8), 1263−1269.
(20) Yan, X.; Zhu, P.; Li, J. Self-Assembly and Application of Diphenylalanine-Based Nanostructures. *Chem. Soc. Rev.* **2010**, *39* (6), 1877−1890.
(21) Hamley, I. W. Peptide Fibrillization. *Angew. Chem., Int. Ed.* **2007**, *46* (43), 8128−8147.
(22) de Loos, M.; Feringa, B. L.; van Esch, J. H. Design and Application of Self-Assembled Low Molecular Weight Hydrogels. *Eur. J. Org. Chem.* **2005**, *2005* (17), 3615−3631.
(23) Raeburn, J.; Cardoso, A. Z.; Adams, D. J. The Importance of The Self-Assembly Process to Control Mechanical Properties of Low Molecular Weight Hydrogels. *Chem. Soc. Rev.* **2013**, *42* (12), 5143−5156.
(24) Ryan, D. M.; Nilsson, B. L. Self-Assembled Amino Acids and Dipeptides As Noncovalent Hydrogels for Tissue Engineering. *Polym. Chem.* **2012**, *3* (1), 18−33.
(25) Ikeda, M.; Tanida, T.; Yoshii, T.; Kurotani, K.; Onogi, S.; Urayama, K.; Hamachi, I. Installing Logic-Gate Responses to A Variety of Biological Substances in Supramolecular Hydrogel-Enzyme Hybrids. *Nat. Chem.* **2014**, *6* (6), 511−518.
(26) Shklyarevskiy, I. O.; Jonkheijm, P.; Christianen, P. C. M.; Schenning, A. P. H. J.; Del Guerzo, A.; Desvergne, J.-P.; Meijer, E. W.; Maan, J. C. Magnetic Alignment of Self-Assembled Anthracene Organogel Fibers. *Langmuir* **2005**, *21* (6), 2108−2112.
(27) Wang, H. M.; Shi, Y.; Wang, L.; Yang, Z. M. Recombinant Proteins As Cross-Linkers for Hydrogelations. *Chem. Soc. Rev.* **2013**, *42* (3), 891−901.
(28) Ziemecka, I.; Koper, G. J. M.; Olive, A. G. L.; van Esch, J. H. Chemical-Gradient Directed Self-Assembly of Hydrogel Fibers. *Soft Matter* **2013**, *9* (5), 1556−1561.
(29) Lowik, D.; Shklyarevskiy, I. O.; Ruizendaal, L.; Christianen, P. C. M.; Maan, J. C.; van Hest, J. C. M. A Highly Ordered Material from Magnetically Aligned Peptide Amphiphile Nanofiber Assemblies. *Adv. Mater.* **2007**, *19* (9), 1191−1195.
(30) Wallace, M.; Cardoso, A. Z.; Frith, W. J.; Iggo, J. A.; Adams, D. J. Magnetically Aligned Supramolecular Hydrogels. *Chem. Eur. J.* **2014**, *20* (50), 16484−16487.
(31) Zhang, S. M.; Greenfield, M. A.; Mata, A.; Palmer, L. C.; Bitton, R.; Mantei, J. R.; Aparicio, C.; de la Cruz, M. O.; Stupp, S. I. A Self-Assembly Pathway to Aligned Monodomain Gels. *Nat. Mater.* **2010**, *9* (7), 594−601.
(32) McClendon, M. T.; Stupp, S. I. Tubular Hydrogels of Circumferentially Aligned Nanofibers to Encapsulate and Orient Vascular Cells. *Biomaterials* **2012**, *33* (23), 5713−5722.
(33) Zhou, J.; Du, X.; Gao, Y.; Shi, J.; Xu, B. Aromatic-Aromatic Interactions Enhance Interfiber Contacts for Enzymatic Formation of A Spontaneously Aligned Supramolecular Hydrogel. *J. Am. Chem. Soc.* **2014**, *136* (8), 2970−2973.
(34) Newcomb, C. J.; Sur, S.; Ortony, J. H.; Lee, O.-S.; Matson, J. B.; Boekhoven, J.; Yu, J. M.; Schatz, G. C.; Stupp, S. I. Cell Death *versus* Cell Survival Instructed by Supramolecular Cohesion of Nanostructures. *Nat. Commun.* **2014**, *5* (1), 3321.
(35) Feng, Z.; Wang, H.; Chen, X.; Xu, B. Self-Assembling Ability Determines The Activity of Enzyme-Instructed Self-Assembly for Inhibiting Cancer Cells. *J. Am. Chem. Soc.* **2017**, *139* (43), 15377−15384.
(36) Feng, Z.; Wang, H.; Wang, S.; Zhang, Q.; Zhang, X.; Rodal, A. A.; Xu, B. Enzymatic Assemblies Disrupt The Membrane and Target Endoplasmic Reticulum for Selective Cancer Cell Death. *J. Am. Chem. Soc.* **2018**, *140* (30), 9566−9573.
(37) Tanaka, A.; Fukuoka, Y.; Morimoto, Y.; Honjo, T.; Koda, D.; Goto, M.; Maruyama, T. Cancer Cell Death Induced by The Intracellular Self-Assembly of An Enzyme-Responsive Supramolecular Gelator. *J. Am. Chem. Soc.* **2015**, *137* (2), 770−775.
(38) Christoff-Tempesta, T.; Cho, Y.; Kim, D.-Y.; Geri, M.; Lamour, G.; Lew, A. J.; Zuo, X.; Lindemann, W. R.; Ortony, J. H. Self-Assembly of Aramid Amphiphiles into Ultra-Stable Nanoribbons and Aligned Nanoribbon Threads. *Nat. Nanotechnol.* **2021**, *16* (4), 447−454.
(39) Acar, H.; Samaeekia, R.; Schnorenberg, M. R.; Sasmal, D. K.; Huang, J.; Tirrell, M. V.; LaBelle, J. L. Cathepsin-Mediated Cleavage of Peptides from Peptide Amphiphiles Leads to Enhanced Intracellular Peptide Accumulation. *Bioconjugate Chem.* **2017**, *28* (9), 2316−2326.
(40) Black, M.; Trent, A.; Kostenko, Y.; Lee, J. S.; Olive, C.; Tirrell, M. Self-Assembled Peptide Amphiphile Micelles Containing A Cytotoxic T-Cell Epitope Promote A Protective Immune Response *in Vivo*. *Adv. Mater.* **2012**, *24* (28), 3845−3849.
(41) Missirlis, D.; Krogstad, D. V.; Tirrell, M. Internalization of $p53_{14-29}$ Peptide Amphiphiles and Subsequent Endosomal Disruption Results in SJSA-1 Cell Death. *Mol. Pharmaceutics* **2010**, *7* (6), 2173−2184.
(42) Álvarez, Z.; Kolberg-Edelbrock, A. N.; Sasselli, I. R.; Ortega, J. A.; Qiu, R.; Syrgiannis, Z.; Mirau, P. A.; Chen, F.; Chin, S. M.; Weigand, S.; Kiskinis, E.; Stupp, S. I. Bioactive Scaffolds with Enhanced Supramolecular Motion Promote Recovery from Spinal Cord Injury. *Science* **2021**, *374* (6569), 848−856.
(43) Sather, N. A.; Sai, H.; Sasselli, I. R.; Sato, K.; Ji, W.; Synatschke, C. V.; Zambrotta, R. T.; Edelbrock, J. F.; Kohlmeyer, R. R.; Hardin, J. O.; Berrigan, J. D.; Durstock, M. F.; Mirau, P.; Stupp, S. I. 3D Printing

https://doi.org/10.1021/acsnano.1c09860
ACS Nano 2022, 16, 4126−4138

of Supramolecular Polymer Hydrogels with Hierarchical Structure. *Small* **2021**, *17* (5), 2005743.
(44) Reches, M.; Gazit, E. Casting Metal Nanowires within Discrete Self-Assembled Peptide Nanotubes. *Science* **2003**, *300* (5619), 625–627.
(45) Fichman, G.; Gazit, E. Self-Assembly of Short Peptides to Form Hydrogels: Design of Building Blocks, Physical Properties and Technological Applications. *Acta Biomater.* **2014**, *10* (4), 1671–1682.
(46) Tena-Solsona, M.; Alonso-de Castro, S.; Miravet, J. F.; Escuder, B. Co-Assembly of Tetrapeptides into Complex pH-Responsive Molecular Hydrogel Networks. *J. Mater. Chem. B* **2014**, *2* (37), 6192–6197.
(47) Panja, S.; Shebanova, O.; Smith, A.; Dietrich, B.; Adams, D. J. Programming Gels over A Wide pH Range using Multicomponent Systems. *Angew. Chem., Int. Ed.* **2021**, *133*, 10061.
(48) Wang, F.; Ji, W.; Yang, P.; Feng, C.-L. Inversion of Circularly Polarized Luminescence of Nanofibrous Hydrogels through Co-Assembly with Achiral Coumarin Derivatives. *ACS Nano* **2019**, *13* (6), 7281–7290.
(49) Swanekamp, R. J.; DiMaio, J. T.; Bowerman, C. J.; Nilsson, B. L. Coassembly of Enantiomeric Amphipathic Peptides into Amyloid-Inspired Rippled β-Sheet Fibrils. *J. Am. Chem. Soc.* **2012**, *134* (12), 5556–5559.
(50) Mohammed, A.; Miller, A. F.; Saiani, A. 3D Networks from Self-Assembling Ionic-Complementary Octa-Peptides. *Macromol. Symp.* **2007**, *251* (1), 88–95.
(51) Marini, D. M.; Hwang, W.; Lauffenburger, D. A.; Zhang, S.; Kamm, R. D. Left-Handed Helical Ribbon Intermediates in The Self-Assembly of A β-Sheet Peptide. *Nano Lett.* **2002**, *2* (4), 295–299.
(52) Warshel, A. Energetics of Enzyme Catalysis. *Proc. Natl. Acad. Sci. U. S. A.* **1978**, *75* (11), 5250–5254.
(53) Barrozo, A.; Duarte, F.; Bauer, P.; Carvalho, A. T. P.; Kamerlin, S. C. L. Cooperative Electrostatic Interactions Drive Functional Evolution in The Alkaline Phosphatase Superfamily. *J. Am. Chem. Soc.* **2015**, *137* (28), 9061–9076.
(54) Daamen, W. F.; Veerkamp, J. H.; van Hest, J. C. M.; van Kuppevelt, T. H. Elastin As A Biomaterial for Tissue Engineering. *Biomaterials* **2007**, *28* (30), 4378–4398.
(55) Kapoor, S.; Kundu, S. C. Silk Protein-Based Hydrogels: Promising Advanced Materials for Biomedical Applications. *Acta Biomater.* **2016**, *31*, 17–32.
(56) Wester, J. R.; Lewis, J. A.; Freeman, R.; Sai, H.; Palmer, L. C.; Henrich, S. E.; Stupp, S. I. Supramolecular Exchange among Assemblies of Opposite Charge Leads to Hierarchical Structures. *J. Am. Chem. Soc.* **2020**, *142* (28), 12216–12225.
(57) Raeburn, J.; Zamith Cardoso, A.; Adams, D. J. The Importance of The Self-Assembly Process to Control Mechanical Properties of Low Molecular Weight Hydrogels. *Chem. Soc. Rev.* **2013**, *42* (12), 5143–5156.
(58) Taraban, M. B.; Feng, Y.; Hammouda, B.; Hyland, L. L.; Yu, Y. B. Chirality-Mediated Mechanical and Structural Properties of Oligopeptide Hydrogels. *Chem. Mater.* **2012**, *24* (12), 2299–2310.
(59) Dong, H.; Paramonov, S. E.; Aulisa, L.; Bakota, E. L.; Hartgerink, J. D. Self-Assembly of Multidomain Peptides: Balancing Molecular Frustration Controls Conformation and Nanostructure. *J. Am. Chem. Soc.* **2007**, *129* (41), 12468–12472.
(60) Huang, S.-C.; Xia, X.-X.; Fan, R.-X.; Qian, Z.-G. Programmable Electrostatic Interactions Expand The Landscape of Dynamic Functional Hydrogels. *Chem. Mater.* **2020**, *32* (5), 1937–1945.
(61) Sun, T. L.; Kurokawa, T.; Kuroda, S.; Ihsan, A. B.; Akasaki, T.; Sato, K.; Haque, M. A.; Nakajima, T.; Gong, J. P. Physical Hydrogels Composed of Polyampholytes Demonstrate High Toughness and Viscoelasticity. *Nat. Mater.* **2013**, *12* (10), 932–937.
(62) Mears, L. L. E.; Draper, E. R.; Castilla, A. M.; Su, H.; Zhuola; Dietrich, B.; Nolan, M. C.; Smith, G. N.; Doutch, J.; Rogers, S.; Akhtar, R.; Cui, H.; Adams, D. J. Drying Affects The Fiber Network in Low Molecular Weight Hydrogels. *Biomacromolecules* **2017**, *18* (11), 3531–3540.
(63) Tena-Solsona, M.; Miravet, J. F.; Escuder, B. Tetrapeptidic Molecular Hydrogels: Self-Assembly and Co-Aggregation with Amyloid Fragment Aβ1–40. *Chemistry* **2014**, *20* (4), 1023–1031.
(64) Sahoo, J. K.; VandenBerg, M. A.; Ruiz Bello, E. E.; Nazareth, C. D.; Webber, M. J. Electrostatic-Driven Self-Sorting and Nanostructure Speciation in Self-Assembling Tetrapeptides. *Nanoscale* **2019**, *11* (35), 16534–16543.
(65) Greenfield, N. J. Using Circular Dichroism Spectra to Estimate Protein Secondary Structure. *Nat. Protoc.* **2006**, *1* (6), 2876–2890.
(66) Holloway, P. W.; Mantsch, H. H. Infrared Spectroscopic Analysis of Salt Bridge Formation between Cytochrome b5 and Cytochrome c. *Biochemistry* **1988**, *27* (21), 7991–7993.
(67) Arunkumar, R.; Drummond, C. J.; Greaves, T. L. FTIR Spectroscopic Study of The Secondary Structure of Globular Proteins in Aqueous Protic Ionic Liquids. *Front. Chem.* **2019**, *7*, 74.
(68) Meuzelaar, H.; Tros, M.; Huerta-Viga, A.; van Dijk, C. N.; Vreede, J.; Woutersen, S. Solvent-Exposed Salt Bridges Influence The Kinetics of α-Helix Folding and Unfolding. *J. Phys. Chem. Lett.* **2014**, *5* (5), 900–904.
(69) Behanna, H. A.; Donners, J. J.; Gordon, A. C.; Stupp, S. I. Coassembly of Amphiphiles with Opposite Peptide Polarities into Nanofibers. *J. Am. Chem. Soc.* **2005**, *127* (4), 1193–1200.
(70) Müller-Buschbaum, P. The Active Layer Morphology of Organic Solar Cells Probed with Grazing Incidence Scattering Techniques. *Adv. Mater.* **2014**, *26* (46), 7692–7709.
(71) Tassler, S.; Pawlowska, D.; Janich, C.; Giselbrecht, J.; Drescher, S.; Langner, A.; Wolk, C.; Brezesinski, G. Lysine-Based Amino-Functionalized Lipids for Gene Transfection: 3D Phase Behaviour and Transfection Performance. *Phys. Chem. Chem. Phys.* **2018**, *20* (25), 17393–17405.
(72) Datar, A.; Balakrishnan, K.; Zang, L. One-Dimensional Self-Assembly of A Water Soluble Perylene Diimide Molecule by pH Triggered Hydrogelation. *Chem. Commun.* **2013**, *49* (61), 6894–6896.
(73) Oldenbourg, R.; Salmon, E. D.; Tran, P. T. Birefringence of Single and Bundled Microtubules. *Biophys. J.* **1998**, *74* (1), 645–654.
(74) Yuan, C.; Ji, W.; Xing, R.; Li, J.; Gazit, E.; Yan, X. Hierarchically Oriented Organization in Supramolecular Peptide Crystals. *Nat. Rev. Chem.* **2019**, *3* (10), 567–588.
(75) Nowak, A. P.; Breedveld, V.; Pakstis, L.; Ozbas, B.; Pine, D. J.; Pochan, D.; Deming, T. J. Rapidly Recovering Hydrogel Scaffolds from Self-Assembling Diblock Copolypeptide Amphiphiles. *Nature* **2002**, *417* (6887), 424–428.
(76) Yang, Z.; He, Y.; Lee, J. H.; Park, N.; Suh, M.; Chae, W. S.; Cao, J.; Peng, X.; Jung, H.; Kang, C.; Kim, J. S. A Self-Calibrating Bipartite Viscosity Sensor for Mitochondria. *J. Am. Chem. Soc.* **2013**, *135* (24), 9181–9185.
(77) Miller, S. E.; Yamada, Y.; Patel, N.; Suarez, E.; Andrews, C.; Tau, S.; Luke, B. T.; Cachau, R. E.; Schneider, J. P. Electrostatically Driven Guanidinium Interaction Domains That Control Hydrogel-Mediated Protein Delivery *in Vivo*. *ACS Cent. Sci.* **2019**, *5* (11), 1750–1759.
(78) Frederix, P. W.; Scott, G. G.; Abul-Haija, Y. M.; Kalafatovic, D.; Pappas, C. G.; Javid, N.; Hunt, N. T.; Ulijn, R. V.; Tuttle, T. Exploring The Sequence Space for (Tri-)Peptide Self-Assembly to Design and Discover New Hydrogels. *Nat. Chem.* **2015**, *7* (1), 30–37.
(79) Draper, E. R.; Eden, E. G. B.; McDonald, T. O.; Adams, D. J. Spatially Resolved Multicomponent Gels. *Nat. Chem.* **2015**, *7* (10), 848–853.
(80) Smith, D. J.; Brat, G. A.; Medina, S. H.; Tong, D. D.; Huang, Y.; Grahammer, J.; Furtmuller, G. J.; Oh, B. C.; Nagy-Smith, K. J.; Walczak, P.; Brandacher, G.; Schneider, J. P. A Multiphase Transitioning Peptide Hydrogel for Suturing Ultrasmall Vessels. *Nat. Nanotechnol.* **2016**, *11* (1), 95–102.

https://doi.org/10.1021/acsnano.1c09860
ACS Nano 2022, 16, 4126–4138